Time-delay control of reversible electron spirals using arbitrarily chirped attosecond pulses

M. A. H. B. Md Yusoff and J. M. Ngoko Djiokap
Department of Physics and Astronomy, University of Nebraska, Lincoln, Nebraska 68588-0299, USA

(Received 20 October 2023; accepted 11 January 2024; published 5 February 2024)

Photoionization through single-photon absorption by two synchronous, linearly chirped, oppositely circularly polarized, attosecond pulses is known [N. J. Strandquist, Jr., and J. M. Ngoko Djiokap, Phys. Rev. A **106**, 043110 (2022)] to create reversible spiral patterns in the momentum distribution of the ejected electron when the two pulses have equal but opposite chirp rates. Here we extend this study by demonstrating how this reversible spiral pattern can be controlled by varying the chirp rates as well as the time delay between the pulses. For two synchronous pulses, we find that using arbitrary chirp rates for each attosecond pulse can create a reversible spiral pattern identical to the one produced by equal but opposite chirp rates when adjusting the carrier-envelope phase difference. By adding a nonzero time delay between the two pulses, we show that the reversible spiral pattern can be controlled by using the accumulated linear Ramsey spectral phase to manipulate the chirp-induced linear or quadratic spectral phases of the photoelectron. Possible applications of such exquisite manipulation of both linear and quadratic spectral phases include manipulation of the photoelectron wave packet group delay.

DOI: 10.1103/PhysRevA.109.023107

I. INTRODUCTION

Spatial two-slit experiments are a cornerstone of interferometry in quantum mechanics and optics. Their temporal counterparts constitute Ramsey interferometry [1] and have been widely studied in atomic systems using linearly polarized laser pulses [2–9] or circularly polarized attosecond laser pulses [10–14]. In the case of linear polarization, Ramsey interference of wave packets producing electrons in Rydberg states [2,4] and in the continuum [5] have been demonstrated experimentally. The 2002 seminal work [5] made use of a sequence of two femtosecond laser pulses to multiphoton ionize potassium atoms. The advent of train [15] or isolated attosecond pulses [16,17] has aroused a tremendous interest in studying, manipulating, and controlling electronic wave packets through Ramsey interference [1]. L'Huillier and collaborators conducted single-photon ionization experiments in argon atoms using a sequence of two attosecond pulses separated by half the infrared laser cycle [7], as well as a train of multiple attopulses [8].

In the case of circular polarization, for broad bandwidths—characteristic of attopulses—capable to support several Ramsey fringes, Ngoko Djiokap *et al.* discovered the *Archimedean irreversible spiral* interferogram in the photoelectron momentum distribution (PMD) in the laser polarization plane following single-photon [10] or multiphoton [11] ionization of helium atoms by a pair of time-delayed, oppositely circularly polarized, copropagating attosecond pulses. The predictions for these attopump-attopump processes [10,11] later confirmed experimentally by the Wollenhaupt group (see, e.g., [12,13]) in the femtosecond regime, have opened up a new research subfield for searches and applications of this key pattern from different processes, regimes, targets, and laser polarization configurations.

Although isolated attopulses [15–21] with full control of their polarization [21] state do exist, the experimental demonstration of these predictions for both the attopump-attopump linear [10] and nonlinear [11] processes in the attosecond regime, as well as the holy grail (attopump-attoprobe nonlinear processes) of attosecond science, is not yet a reality. Indeed, current methods for producing an isolated attopulse, either from the nonlinear process of high-order harmonic generation within the XUV region [15–21] or from free-electron lasers within the soft x-ray spectral region [22], always introduce an intrinsic chirp called an attochirp, i.e., a time-dependent laser pulse carrier frequency. This chirp decreases the isolated attopulse intensity and broadens its duration (but keeps its bandwidth unchanged). The weak intensity combined with a lack of carrier-envelope phase stabilization render difficult any realization of the holy grail so far, while the measurement of the spiral interferogram requires copropagating attopulses with broad bandwidth characteristic of transform-limited pulses (TLPs). To achieve the main goal of attosecond science by using an isolated attopulse to better control electronic motion [23], it is crucial to examine whether and how attochirp influences the PMDs produced from both linear and nonlinear ionization processes. Just like carrier-envelope phase effects, while the chirp of a single laser pulse is known to affect nonlinear ionization processes [24–41], no chirp effects are expected for linear ionization processes starting from the ground state (not a superposition of states like in [42]) within the rotating-wave approximation (RWA).

It is within this context that we previously investigated the linear process of single-photon single ionization of He produced by a pair of synchronous, oppositely circularly polarized attopulses with equal and opposite chirp rates and identified a new type of spiral interferogram. Because of its energy-dependent handedness, it was dubbed *reversible spiral* [43]. Not only was the sense of rotation of such spirals found to depend on the pulse helicities, it also has a dependence on the sign of the chirp-rate difference. This behavior of

reversible spirals can be traced from the chirp-induced linear and quadratic spectral phase accumulated between the simultaneous creation of the two-electron wave packets in the continuum. In contrast, *irreversible spirals* [10–13] can be traced from the Ramsey linear spectral phase accumulated between the creation of the two-electron wave packets in the continuum with a time delay. For reversible spiral patterns predicted in 2022 [43]—which has just been confirmed experimentally in 2023 but in the femtosecond regime by the Wollenhaupt group [44]—to be measured in the attosecond regime, they need to be fully controllable. This can be achieved by tuning the amount of chirp inside the laser pulse while eventually delaying in time the two ionizing attopulses, as considered in this contribution. Such a control scheme provides a great possibility of investigating or comparing the shapes of the PMDs produced by electric fields, whose components in the polarization plane can be viewed as temporal single slit or double slits.

In this paper we examine the linear process of single-photon single ionization of an S-state atom using a pair of oppositely circularly polarized laser pulses with a focus on the chirp nature of the pulse electromagnetic radiations while they are temporally separated eventually. Because the investigation [43] was restricted to the case of equal and opposite chirp rates with zero time delay, the present investigation is a natural extension of the study [43] to the case where isolated attopulses with arbitrary chirped rates are used with eventually nonzero time delay. Although the perturbation theory (PT) for single-electron ionization holds for any S-state atom (H, He, etc.), we restrict the presentation of our numerical time-dependent Schrödinger equation (TDSE) results to the case of helium atom, because it was previously used in [43] and it is more easily handled experimentally than hydrogen atom. Our findings are threefold:

(i) For two synchronous pulses (i.e., a temporal single slit in the x component and a distorted temporal double slit in the y component of the resulting electric field), we find that using arbitrary chirp rates for each attosecond pulse can create a reversible spiral pattern identical to the one produced by equal but opposite chirp rates for the same chirp-rate difference $\Delta\xi$ when properly tuning the carrier-envelope phase difference. For fixed helicities of the oppositely circularly polarized pulses, the energy-dependent spiral handedness is determined by the sign of $\Delta\xi$.

By temporally delaying the two attopulses, the shape of the reversible spiral pattern can be transformed using the accumulated time-delay–induced linear Ramsey spectral phase to manipulate the chirp-induced linear or quadratic spectral phases of the photoelectron. There are two key results of interest reported here.

(ii) For $\Delta\xi > 0$, we find that the time delay strengthens the linear spectral phase, thus causing the spiral pattern due to the linear phase term to dominate even in the high-energy region. This transforms the reversible spiral to an irreversible one with broader spiral-arm widths as the photoelectron energy increases.

(iii) For $\Delta\xi < 0$, the time delay weakens the linear spectral phase, and the obtained reversible spirals are not the symmetrical mirror image of the irreversible spiral produced for $\Delta\xi > 0$ with the same $|\Delta\xi|$. When the time delay is present, mirroring effects can only be seen now when flipping the pulse helicities at a fixed $\Delta\xi$. We determine the critical time delay τ_c for which the total linear spectral phase vanishes, since the linear spectral phase components from chirp (with $\Delta\xi < 0$) and time delay balance each other. Taking this time delay τ_c allows us to isolate a tightly wound irreversible (not reversible) spiral pattern stemming from linear and quadratic spectral phases with the same sign.

This paper is organized as follows. In Sec. II we describe our numerical methods for solving the full dimensional TDSE together with a parametrization of the chirped, oppositely circularly polarized isolated attopulses. In Sec. III we present our numerical TDSE results, which are analyzed using first-order PT. Finally, Sec. IV is devoted to some concluding remarks. Throughout this work, atomic units are used unless stated otherwise.

II. NUMERICAL METHODS

We begin our investigation by considering the interaction of the helium atom in its $^1S^e$ ground state with the electric field $\mathbf{F}(t)$ of a pair of oppositely circularly polarized attopulses with the same carrier frequency ω_0, but maybe differing in their carrier-envelope phases $\phi_{1,2}$ and chirp rates $\xi_{1,2}$. These two pulses may be delayed in time by τ. Throughout this work we focus on the process of photoionization, i.e., single ionization by a single photon absorption, with the observable of interest being the PMD. We parametrize the electric field as

$$\mathbf{F}(t) = F_1(t)\,\mathrm{Re}\,\{\mathbf{e}_1 e^{-i[\omega_1(t)t+\phi_1]}\} + F_2(t-\tau)\,\mathrm{Re}\,\{\mathbf{e}_2 e^{-i[\omega_2(t)(t-\tau)+\phi_2]}\}, \quad (1)$$

where for the jth pulse ($j = 1, 2$) with carrier-envelope phase ϕ_j, $\mathbf{e}_j \equiv (\hat{\mathbf{x}} + i\eta_j\hat{\mathbf{y}})/(1+\eta_j^2)^{1/2}$ is the polarization vector. The unit vectors $\hat{\mathbf{x}}$ and $\hat{\mathbf{y}}$ define the major and minor axes, respectively, of the polarization ellipse, while the laser pulse is propagating along the $\hat{\mathbf{z}}$ axis. The quantity $|\eta_j|$ is the ellipticity in which $-1 \leqslant \eta_j \leqslant 1$ [33]. For linear polarization, one has $|\eta_j| = 0$, while for circular polarization (CP), one has $|\eta_j| = 1$. Here the sign of η_j defines the helicity, where for the jth pulse, $\eta_j = +1(-1)$ for the right (left) circularly polarized attopulses, abbreviated as RCP (LCP).

A pulse is said to be chirped when its instantaneous carrier frequency is time dependent [47]. For a linearly chirped pulse, the carrier frequency of the jth pulse can be mathematically expressed as

$$\omega_j = \omega_0 + 2\ln 2\,\frac{\xi_j}{1+\xi_j^2}\,\frac{t}{\tau_0^2} \equiv \omega_0 + b_j t, \quad (2)$$

where the quantity ξ_j is the dimensionless chirp rate, which can be controlled as described in [23] or by propagating the pulse through a dispersive media with thickness d_j and group velocity dispersion k_j'', where $\phi_j'' = k_j'' d_j = \xi_j\tau_0^2/4\ln 2$ [37,46,47] is the group delay dispersion [37,45–47]. The dimensionless chirp rate can be positive (up-chirp), where it would increase the carrier frequency. It can also be negative (down-chirp), where it would decrease the carrier frequency of the attopulses as time goes on. Here, $I_0 = F_0^2$, τ_0, and

ω_0 are respectively the peak intensity, duration (FWHM) of the intensity profile, and central carrier frequency of the corresponding TLP. The functions $F_1(t)$ and $F_2(t-\tau)$ in Eq. (1) are the Gaussian envelope, defined as $F_j(t) = \sqrt{I_j}\exp(-2\ln 2\frac{t^2}{\tau_j^2})$ for $j = 1, 2$, and involving the peak intensity,

$$I_j = I_0/\sqrt{1+\xi_j^2}, \tag{3}$$

and the duration of the intensity profile,

$$\tau_j = \tau_0\sqrt{1+\xi_j^2}. \tag{4}$$

Since the chirp extends the effective pulse duration as demonstrated in (4), to maintain equivalent total energy with the chirp-free case the peak intensity is reduced by the same amount $(1+\xi_j^2)^{1/2}$ as demonstrated in (3). This allows for a transparent comparison between the chirped and chirp-free cases [43], as well as between the case of equal and opposite chirp rates and the case of arbitrary chirp rates discussed here. For pedagogical reasons, we use the same pulse parameters as in [43]: a central carrier frequency $\omega_0 = 36\,\text{eV}$, a peak intensity $I_0 = 10^{14}\,\text{W/cm}^2$, and a pulse duration (FWHM) in the intensity profile $\tau_0 = 243$ as corresponding to three optical cycles.

To numerically calculate the triply differential probability (TDP) for the photoionization process, we numerically solve the following seven-dimensional two-electron TDSE in the length gauge,

$$i\frac{\partial}{\partial t}\Phi(\mathbf{r_1}, \mathbf{r_2}, t) = H(t)\Phi(\mathbf{r_1}, \mathbf{r_2}, t), \tag{5}$$

to obtain the electron wave packet at the end of the laser pulse duration $t = T_f$, where $H(t) = H_0 + \mathbf{d}\cdot\mathbf{F}(t)$ includes the field-free two-electron Hamiltonian H_0 and the laser-atom interaction term $\mathbf{d}\cdot\mathbf{F}(t)$ within the electric dipole approximation, with $\mathbf{d} = \mathbf{r_1} + \mathbf{r_2}$ being the electric dipole moment operator and $\mathbf{F}(t)$ being the electric field given by Eq. (1).

To solve the seven-dimensional (including time) two-electron TDSE, we adopt a close-coupling approach first introduced in [48,49], which consists of expanding the two-electron wave function $\Phi(\mathbf{r_1}, \mathbf{r_2}, t)$ onto the basis of bipolar spherical harmonics $\Lambda^{LM}_{l_1,l_2}(\hat{r}_1, \hat{r}_2)$:

$$\Phi(\mathbf{r_1}, \mathbf{r_2}, t) = \sum_{LM}\sum_{l_1 l_2}\frac{\psi^{LM}_{l_1 l_2}(r_1, r_2, t)}{r_1 r_2}\Lambda^{LM}_{l_1,l_2}(\hat{r}_1, \hat{r}_2). \tag{6}$$

Such close-coupling expansion reduces the complexity of the problem from seven dimensions to three dimensions, as reflected by the number of variables in the argument of the expansion coefficient $\psi^{LM}_{l_1 l_2}(r_1, r_2, t)$. This is possible because the bipolar spherical harmonics involve the four dimensions of the solid angles $(\hat{r}_1, \hat{r}_2)$ of the two electrons. To discretize the radial wave function $\psi^{LM}_{l_1 l_2}(r_1, r_2, t)$, we use a fine-gridding scheme of finite-element, discrete-variable representation first introduced in [50]. We used a two-dimensional grid ranging to a maximum of 120 Bohr radius, which is spanned by 60 finite elements with an equal size of 2 Bohr radius. Within each finite element, an eight-point Gauss-Legendre-Lobatto basis is used. To time propagate the wave function $\psi^{LM}_{l_1 l_2}(r_1, r_2, t)$, we employ the real-space-product algorithm (a variant of the split-operator method) [51–54]. To treat the complicated M-mixing problem [55] introduced by the use of circular polarization, we adopt the basic principle of the method introduced by Muller [56] and developed further in [10,11,55,57–59]. At each time step we introduce two frames: the laboratory frame in which we treat the atomic interaction and the rotating frame of the instantaneous electric field in which we treat the laser-matter interaction. The passage from one frame to another is done by means of Wigner rotation transformation that deals analytically with the M-mixing problem and thus speeds up the numerical computation. The rationale behind this procedure is that the electric field seen by an observer in the rotating frame is always linearly polarized. This procedure is very accurate for small time steps, which is guaranteed throughout this work. In our photoionization calculations, we include four total angular momentum ($L = 0-3$) of the two electrons—the azimuthal total angular momentum $|M| \leqslant L$ and all possible combinations of each electron angular momentum $l_1 = 0-5$ and $l_2 = 0-5$. At $t = T_f$, i.e., at the end of the laser pulse, we project the wave function $\Psi(\mathbf{r_1}, \mathbf{r_2}, T_f)$, the solution of the TDSE, onto a field-free scattering wave function as prescribed in [60]:

$$\mathcal{W}(\mathbf{p}) = |\langle\Theta^{(-)}_{\mathbf{1s},\mathbf{p}}(\mathbf{r_1}, \mathbf{r_2})|\Phi(\mathbf{r_1}, \mathbf{r_2}, T_f)\rangle|^2. \tag{7}$$

Here, the field-free scattering state $\Theta^{(-)}_{\mathbf{1s},\mathbf{p}}(\mathbf{r_1}, \mathbf{r_2})$, for our single ionization without excitation channel, where the photoelectron in the continuum with momentum $\mathbf{p} \equiv (p, \theta, \varphi)$ and the residual helium ion remaining in its $1s$ ground state are constructed using the Jacobi matrix method [52]. For large chirp rates, the effective pulse duration increases significantly. Thus it is important that the TDSE be solved for long enough time T_f given the long-tail nature of the Gaussian envelope. For the typical pulse parameters used throughout this paper, converged results for the TDP are obtained.

III. ANALYTICAL AND NUMERICAL RESULTS

For pulse parameters used throughout this work, the Keldysh parameter γ is about 33 and the electron ponderomotive energy U_p of 0.011 eV is very small compared to $\omega_0 = 36\,\text{eV}$. The implication is that we are in the perturbative multiphoton regime, where the time-dependent PT is applicable. To understand the TDSE numerical results for the TDP for the following photoelectron energy range $0 \leqslant E \leqslant 30\,\text{eV}$ presented below in Sec. III B for the case of equal and opposite chirp rates at $\tau = 0$, in Sec. III C for the case of arbitrary chirp rates at $\tau = 0$, and in Sec. III D for the case of equal and opposite chirp rates at nonzero time delays, we employ the first-order PT framework with the TDP being calculated analytically as $\mathcal{W}(\mathbf{p}) = |A|^2$. Here, the transition amplitude A is given by [61]

$$A = -i\int_{-\infty}^{\infty} e^{+iE_f t}\langle\Psi^{(-)}_{\nu\mathbf{p}}|\mathbf{d}\cdot\mathbf{F}|i\rangle e^{-iE_i t}dt, \tag{8}$$

where $|\Psi^{(-)}_{\nu\mathbf{p}}\rangle$ is the final state with energy $E_f \equiv E + E_\nu$ satisfying incoming wave boundary conditions [62] and

comprising the bound state ν of the residual ion and the continuum state of the electron with energy $E = p^2/2$; and $|i\rangle$ is the initial state with experimental energy $E_i = -E_g = -2.9037$ a.u., which compares well with our calculated energy of -2.9031 a.u. In terms of the binding energy $E_b = E_\nu + E_g$ of an He atom, one has $E_f - E_i = E + E_b$. Note that the PT transition amplitude (8) describes only single-photon absorption processes. Indeed, for the rather weak laser peak intensity used here, single-photon emission processes are negligible. This means that the analytical evaluation of the amplitude (8) does exclude the c.c. part of the expression of the electric field $\mathbf{F}(t)$ given by Eq. (1). In contrast, the full expression for the electric field $\mathbf{F}(t)$ is used in the TDSE calculation.

A. Electric field analysis in the time domain for synchronous pulses

Before we present our analytical and numerical results for the TDP in the different three cases mentioned above, it is instructive to first inspect the time dependence of the electric field components $F_x(t) = F_{1,x}(t) + F_{2,x}(t)$ and $F_y(t) = F_{1,y}(t) + F_{2,y}(t)$ in the laser polarization plane for some chirp configurations at zero time delay and equal carrier-envelope phases.

For a pair of identically chirped oppositely circularly polarized attopulses, it is obvious that the x components of the electric field add up constructively to produce $F_x(t)$, which exhibits a single unchirped burst of light; while the y components of the electric field cancel out, $F_y(t) = 0$, as illustrated in Fig. 1(a) for the chirp rates $\xi_1 = \xi_2 = +1$. The implication is that the resulting electric field of the pair of identically chirped oppositely circularly polarized attopulses (just like for two oppositely circularly polarized TLPs) is then linearly polarized along the major x axis of the polarization ellipse, meaning that the PMD in the laser polarization plane from this temporal single-slit scheme should exhibit a dipole pattern along the x axis. This prediction, based on the analysis of the electric field, is confirmed by TDSE calculations; see Fig. 1(d) in [43].

For the case of two oppositely circularly polarized attopulses with equal and opposite chirp rates, Eq. (A5) in [43] shows that the x components of the electric field add up constructively to produce a single unchirped burst of light $F_x(t)$, while Eq. (A6) in [43] shows that the y components now overlap to produce two unchirped bursts of light well separated in time, as illustrated in Fig. 1(b) for the chirp rates $\xi_1 = -\xi_2 = +1$. The implication is that there is a temporal single slit along the major axis of the polarization ellipse and a chirp-induced temporal double slit along its minor axis. These observations indicate that the shape of the PMD in the laser polarization plane should strongly differ from the one (dipole pattern discussed above) produced by TLPs or identical chirped pulses from one side and from the one produced by a pair of time-delayed, oppositely circularly polarized TLPs on the other side. In the latter case, each of $F_x(t)$ and $F_y(t)$ are equivalent to a temporal double slit, as each exhibits two bursts of light, and Archimedean spirals emerge in the PMD. Those spirals are coined irreversible

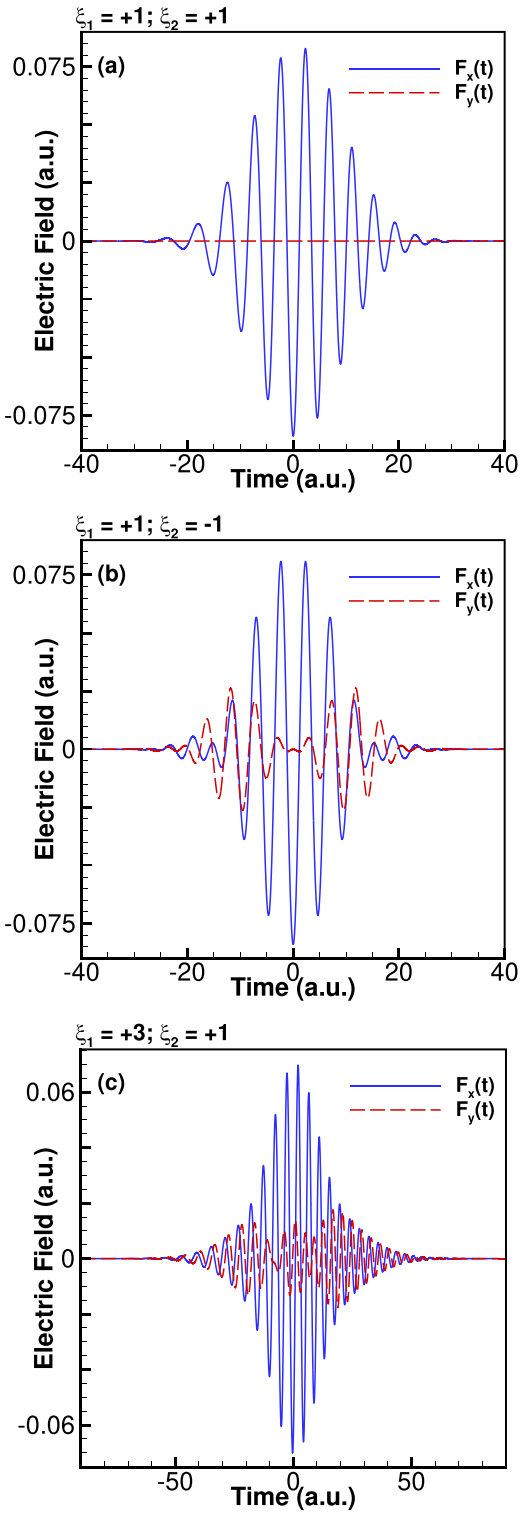

FIG. 1. Time dependence for the electric components, $F_x = F_{1,x} + F_{2,x}$ and $F_y = F_{1,y} + F_{2,y}$, of two synchronous, right-left circularly polarized (RLCP) attopulses for (a) equal chirp rates ($\xi_1 = \xi_2 = 1$), (b) equal but opposite chirp rates ($\xi_1 = -\xi_2 = +1$), and (c) arbitrary chirp rates ($\xi_1 = +3$, $\xi = +1$).

spirals because once the direction of a spiral winding is established by the pulse helicities it is impossible to reverse it. For illustration, Fig. 1(e) in [43] and Fig. 2(a) show an example of this new class of pattern, coined hereafter reversible

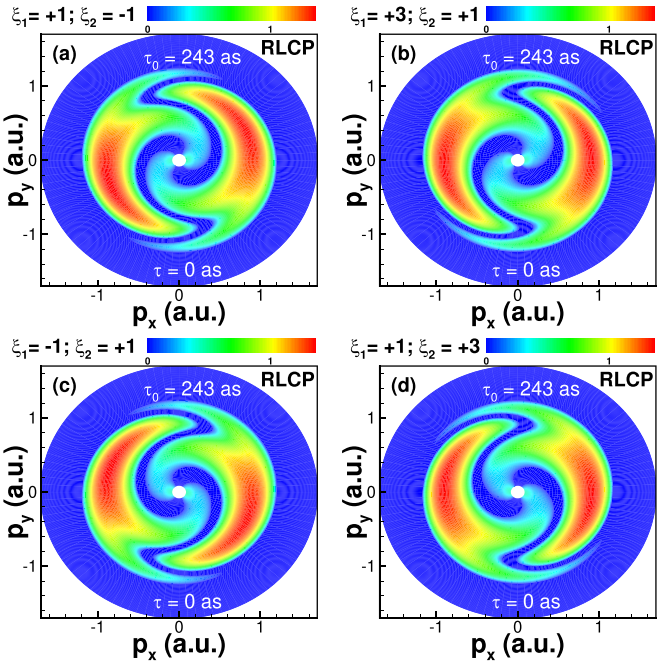

FIG. 2. PMDs in the polarization plane produced by two synchronous (i.e., with zero time delay) right-left circularly polarized (RLCP) pulses for (a) equal and opposite chirp rates ($\xi_1 = 1, \xi_2 = -1$), (b) arbitrary chirp rates $\xi_1 = +3, \xi_2 = +1$, (c) equal and opposite chirp rates $\xi_1 = -1, \xi_2 = +1$, and (d) $\xi_1 = +1, \xi_2 = +3$. The pattern produced in (a) is similar to that in (b) but with a difference in their global rotation. Exchanging the chirp rates of the two attopulses results in PMDs which are mirror images to one another.

spirals given their energy-dependent handedness, as explained later.

In the instructive case where the two oppositely circularly polarized attopulses are arbitrarily chirped (e.g., $\xi_1 = +3$ and $\xi_2 = +1$), despite the difference in both the envelopes and carrier waves, a single unchirped burst of light (i.e., a single slit) in the x component $F_x(t)$ can still be seen in Fig. 1(c) as a result of mixing the two x components of the electric field. It is also seen that the duration of the electric field is extended, while its field strength is reduced. However, the y component of the resulting electric field $F_y(t)$ presents two overlapping irregular bursts of light with significantly reduced nonzero structures in between them, meaning that the concept of time slit is not applicable. Given the dramatic differences in the shape of the electric field component $F_y(t)$ for the equal and opposite chirp case in Fig. 1(b) and the arbitrary chirp case in Fig. 1(c), whether the shapes of the produced PMDs in those two cases with the same chirp-rate difference $\Delta\xi = (\xi_1 - \xi_2)/2 = +1$ can be identical or even similar is a nontrivial question that needs to be elucidated. Below we provide a clear answer to that question using perturbation theory analysis. In Sec. III B, PT predicts that the PMD for the case of oppositely circularly polarized with arbitrary chirp rates produces an interferogram similar to the spiral pattern for the case of oppositely circularly polarized with equal and opposite chirp rates, but they differ only by a global rotation, which can be eliminated using the carrier-envelope phase difference. This prediction turns out to be in concert with the TDSE results.

B. Reversible electron spiral pattern by oppositely circularly polarized pulses with equal and opposite chirp rates at zero time delay

Although this case was the focus of Ref. [43], for pedagogical reasons we provide here a brief overview of these findings, as the structure of the argument of the kinematical factor of the TDP is the main ingredient in grasping the modification brought by the arbitrary nature of the pulses (see Sec. III C). For the case of oppositely circularly polarized pulses with equal and opposite chirps $\xi_1 = -\xi_2 \equiv \xi$, the TDP $\mathcal{W}(\mathbf{p})$ derived in [43] is written

$$\mathcal{W}(\mathbf{p}) = g(p,\theta)\cos^2\left\{\frac{(\Phi+\beta)}{2} - \frac{\tau_0^2(\omega_0-\epsilon)^2\xi}{16\ln 2} - \hat{\eta}\varphi\right\}, \tag{9}$$

where $\mathbf{p} = (p,\theta,\varphi)$ is the photoelectron momentum, and $\Phi = \phi_{12} + (E+E_b)\tau$ is the relative phase involving the Ramsey $(E+E_b)\tau$ and the carrier-envelope phase difference $\phi_{12} = \phi_1 - \phi_2$. Here, $\beta = \arctan(\xi)$ is the chirp-induced phase shift; $\hat{\eta} = +1(-1)$ for RLCP(LRCP) pulses; and we introduce the energy parameter $\epsilon = E + E_b$. The function $g(p,\theta) \equiv g(p)\sin^2(\theta)$ has a dynamical variable $g(p)$ that depends only on the energy of the photoelectron where $E = p^2/2$:

$$g(p) = \frac{I_0\pi\tau_0^2}{8\ln 2}\Upsilon(p)\sin^2\theta\exp\left\{-\frac{(\omega_0-\epsilon)^2\tau_0^2}{2\ln 2}\right\}. \tag{10}$$

The term $\Upsilon(p)$ is the radial matrix element between the ground state and the final state. The pattern of the PMD that emerges in the polarization plane (xy plane, where $\theta = \pi/2$) is described by the zeros and maxima of the argument of the cosine factor in the TDP (9),

$$\varphi^{\max,0}(E) = \hat{\eta}\left\{k\pi + \frac{(\Phi+\beta)}{2} - \frac{\tau_0^2(\omega_0-\epsilon)^2\xi}{16\ln 2}\right\}, \tag{11}$$

where k is an integer for maxima and half-integer for zeros. For the chirp-free case where $\xi = 0$, we see that $\beta = 0$ and Eq. (11) becomes $\varphi^{\max,0}(E) = \hat{\eta}(k\pi + \Phi/2)$. At zero time delay $\tau = 0$, the term Φ now becomes $\Phi = \phi_{1,2}$. As described in [10], the TDP predicts a dipole pattern whose direction is described by $\Phi = \phi_{12}$. When $\phi_{12} = 0$, the dipole pattern is aligned along the major x axis of the polarization ellipse.

Any term with an energy dependence in (11) determines the shape of the PMD. Looking at the case $\xi \neq 0$ while $\tau = 0$, we see from Eq. (11) that the chirp-induced phase shift β as well as $\Phi = \phi_{12}$ only induce a global rotation of the PMD. The only term in Eq. (11) with an energy dependence is its last term, $\propto [\tau_0^2(\omega_0-\epsilon)^2\xi]$, which is induced by the chirp $\xi \equiv \xi_1 = -\xi_2$. This chirp-induced spectral phase produces a reversible spiral pattern in the PMD with two arms because one photon is absorbed from each pulse. The origin of the reversible spiral pattern can be explained quantitatively using the astrophysical concept of pitch angle thoroughly discussed in [43] or qualitatively by expanding the chirp-induced spectral phase, $(\omega_0-\epsilon)^2\tau_0^2\xi$, into three terms $[\omega_0^2 - 2\omega_0\epsilon + \epsilon^2]\tau_0^2\xi$. For a fixed ξ and $\hat{\eta}$, the first term $\omega_0^2\tau_0^2\xi$ will induce a global rotation of the PMD; because the linear

spectral phase $-2\omega_0\epsilon\tau_0^2\xi$ and the quadratic spectral phase $\epsilon^2\tau_0^2\xi$ have opposite signs, they will rotate the dipole pattern to generate spirals in two opposite directions. While the linear spectral phase dominates in the low-energy region and dictates the spiral handedness, the quadratic spectral phase dominates in the high-energy region and is responsible for the change in the sense of rotation. Between low and high energies, the linear and quadratic spectral phases are comparable. Such a reversible pattern is shown in Fig. 2(a) from TDSE calculations for the case $\xi \equiv \xi_1 = -\xi_2 = +1$ at $\tau = 0$, where $\Phi = \phi_{12} = 0$.

C. Reversible electron spiral pattern by arbitrarily chirped, oppositely circularly polarized pulses at zero time delay

For the case where the two attopulses have arbitrary chirp values ξ_1 and ξ_2, and are different in absolute values, the TDP $\mathcal{W}(\mathbf{p})$ in the laser polarization plane ($\theta = \pi/2$) can be written as

$$\mathcal{W}(\mathbf{p}) = g(p,\theta)\cos^2\left\{\frac{(\Phi+\Delta\beta)}{2} - \frac{\tau_0^2(\omega_0-\epsilon)^2\Delta\xi}{16\ln 2} - \hat{\eta}\varphi\right\}. \tag{12}$$

At first glance, one sees that the TDPs in Eqs. (9) and (12) have the same structure, with the only difference being that the chirp-induced phase shift $\beta = \arctan(\xi)$ in (9) is now replaced by the chirp-induced phase-shift difference $\Delta\beta = [\arctan(\xi_1) - \arctan(\xi_2)]/2$ in (12), while the chirp rate ξ in (9) is now replaced by the chirp-rate difference $\Delta\xi = (\xi_1 - \xi_2)/2$ in (12). For equal and opposite chirp rates $\xi \equiv \xi_1 = -\xi_2$, one has $\Delta\xi = (\xi_1 - \xi_2)/2 = \xi$ and $\Delta\beta = [\arctan(\xi_1) - \arctan(\xi_2)]/2 = \arctan(\xi)$, because arctan is an odd function. One sees that in this scheme, the TDP (12) reduces to Eq. (9), as it should be. Therefore, the implication is that reversible spirals are then expected to emerge in the PMD in the polarization plane for the case of arbitrarily chirped, oppositely circularly polarized pulses at zero time delay, as illustrated in Fig. 2(b), where the chirp rates considered are $\xi_1 = +3$ and $\xi_2 = +1$ at $\tau = 0$ and zero carrier-envelope phases. Here, the chirp-rate difference is $\Delta\xi = (\xi_1 - \xi_2)/2 = +1$, which is the same for the equal and opposite chirp rates $\xi \equiv \xi_1 = -\xi_2 = +1$. Inspecting carefully Fig. 2(b) shows that this pattern bears a close resemblance to the pattern in Fig. 2(a), but they differ just by a global rotation. It should be noted that TDSE calculations for the case of arbitrarily chirped, oppositely circularly polarized pulses with large chirp amounts is challenging because of the rather long pulse duration. Only when the TDSE code is propagated long enough in time to account for the long-tail Gaussian envelope are converged results for the TDP obtained.

This tiny difference (global rotation) can be fully understood by comparing the reversible spiral equations for the case

$$\varphi^{\max,0}(E) = \hat{\eta}\left\{k\pi + \frac{(\Phi+\Delta\beta)}{2} - \frac{\tau_0^2(\omega_0-\epsilon)^2\Delta\xi}{16\ln 2}\right\} \tag{13}$$

with those (11) for the case of equal and opposite chirp rates. Indeed, for the case of equal and opposite chirp rates, $\xi \equiv \xi_1 = -\xi_2 = +1$, the chirp-induced phase shift is $\beta = \arctan(\xi) = 45^\circ$, while for the case of arbitrarily chirped, oppositely circularly polarized pulses with $\xi_1 = +3$ and $\xi_2 = +1$, the chirp-induced phase-shift difference is $\Delta\beta = [\arctan(\xi_1) - \arctan(\xi_2)]/2 = 13.3^\circ$. The implication is that a counterclockwise rotation of the PMD in Fig. 2(b) by an angle of $|\Delta\beta - \xi| = 31.7^\circ$ would lead to Fig. 2(a). As all these results were obtained for zero carrier-envelope phases, it turns out that tuning the carrier-envelope phase difference Φ_{12} in the case of arbitrarily chirped, oppositely circularly polarized pulses to cancel the angle $|\Delta\beta - \xi| = 31.7^\circ$ appears as a natural way to control the reversible spirals in Fig. 2(b) in such a way that they will coincide with the pattern in Fig. 2(a). This prescription from PT has been implemented by our TDSE calculation, and this test was satisfactory.

Swapping the chirp rates between the two pulses or the pulse helicities engenders an intriguing phenomenon. Regarding the sense of rotation of the reversible spirals, Eq. (12) or (13) demonstrates that it is dictated by the signs of $\hat{\eta}$ and $\Delta\xi$. For fixed pulse helicities, i.e., $\hat{\eta} = +1$ (RLCP) as is the case in Fig. 2(b), because $\Delta\xi > 0$ one sees a counterclockwise spiral at low energy followed by a clockwise spiral at high energy. Changing the pulse helicities to $\hat{\eta} = -1$ (LRCP) while keeping the same $\Delta\xi$ would lead to a reversible spiral that is a mirror image of the pattern in Fig. 2(b), not shown. Swapping the chirp rates while maintaining the same pulse helicities, one sees that the PMDs for $\xi_1 = +3, \xi_2 = +1$ [see Fig. 2(b)] and $\xi_1 = +1, \xi_2 = +3$ [see Fig. 2(d)] exhibit a symmetrical mirroring effect. Because the case of equal and opposite chirp rates is just a particular case of arbitrary chirp rates, the same phenomenon is observed for $\xi_1 = +1, \xi_2 = -1$ [see Fig. 2(a)] and $\xi_1 = -1, \xi_2 = +1$ [see Fig. 2(c)].

D. Reversible electron spiral pattern by oppositely circularly polarized pulses with equal and opposite chirp rates at nonzero time delay

Since $\Phi = \phi_{12} + (E + E_b)\tau$, having a nonzero time delay τ may be transformative in the sense that the physical picture for the mirroring effect discussed above in Sec. III C can change. Indeed, when the two oppositely circularly polarized pulses with arbitrary chirps are synchronous, mirroring effects occur in the PMD in the laser polarization plane and they are dictated by both the pulse helicities ($\hat{\eta} = \pm 1$) and the sign of chirp-rate difference $\Delta\xi$. Here, when the two pulses are delayed in time we show that such mirroring effects are now only controlled by the pulse helicities. In other words, we show below how flipping the sign of the chirp-rate difference $\Delta\xi$ (while keeping $\hat{\eta}$ fixed) destroys the symmetrical mirroring effects.

The reversible spiral equations (13) can be expanded to take the following form:

$$\varphi^{\max,0}(E) = \hat{\eta}\left\{k\pi + \frac{(\phi_{1,2}+\Delta\beta)}{2} - \frac{\tau_0^2\omega_0^2\Delta\xi}{16\ln 2}\right\} + \hat{\eta}\left\{\left(\frac{\tau}{2} + \frac{2\tau_0^2\omega_0\Delta\xi}{16\ln 2}\right)\epsilon - \frac{\tau_0^2\Delta\xi}{16\ln 2}\epsilon^2\right\}, \tag{14}$$

where we have grouped together the energy-independent terms and the energy-dependent terms. In the right-hand side of Eq. (14), its second term presents a linear energy-dependent

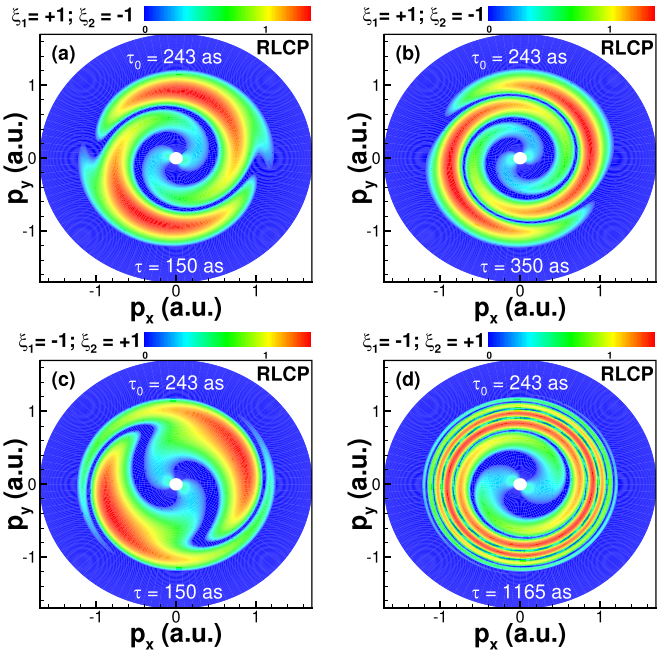

FIG. 3. PMDs in the polarization plane produced by a pair of time-delayed RLCP pulses for (a) equal and opposite chirp rates $\xi_1 = +1, \xi_2 = -1$ at a time delay $\tau = 150$ as, (b) $\xi_1 = +1, \xi_2 = -1$ at a time delay $\tau = 350$ as, (c) $\xi_1 = -1, \xi_2 = +1$ at a time delay $\tau = 150$ as, and (d) $\xi_1 = -1, \xi_2 = +1$ at the critical time delay $\tau_c = 1.165$ fs, see text.

term and a quadratic energy-dependent term with opposite signs. Note that only the linear energy-dependent term has an explicit dependence on the time delay τ. Since the linear spectral phase dominates in the low-energy region while the quadratic spectral phase dominates in the high-energy region, delaying the two oppositely circularly polarized pulses in time can either strengthen or weaken the linear energy-dependent term depending upon the sign of $\Delta\xi$. When $\Delta\xi > 0$, the time delay strengthens the linear term, making the spiral pattern due to the linear spectral phase dominate even at high energy. We tested this PT prediction using our TDSE calculations. The obtained results for $\xi_1 = -\xi_2 = +1$ at time delays $\tau = 150$ as [see Fig. 3(a)] and $\tau = 350$ as [see Fig. 3(b)] can be compared with the reference result at $\tau = 0$ [see Fig. 2(a)]. One sees that the clockwise spiral pattern (known to be due to the quadratic spectral phase) clearly visible in Fig. 2(a) at high energy fades out with increasing the time delay, while a counterclockwise spiral pattern (known to be due to the linear spectral phase) fades in. Thus, the reversible spiral produced by two synchronous, oppositely circularly polarized pulses is now transformed to an irreversible spiral when the two pulses are significantly delayed in time. For the case of $\Delta\xi < 0$, Eq. (14) shows that the time delay weakens the linear term. To show this numerically, we present in Fig. 3(c) our TDSE results for the same pulse parameters as in Fig. 3(a) (e.g., $\tau = 150$ as) but for swapped chirp rates (i.e., $\xi_1 = -\xi_2 = -1$). Comparing Figs. 3(a) and 3(c) for equal but opposite $\Delta\xi$ at the same time delay $\tau = 150$ as, one sees that they are very different. While Fig. 3(c) exhibits a clear reversible spiral, Fig. 3(a) presents almost an irreversible spiral (as some little trace of the quadratic spectral phase is still visible at high energy for such small time delay). Although the two patterns have an opposite sense of rotation, it is clear that they are not mirror images of one another. Regardless of the sign of the chirp-rate difference $\Delta\xi$, TDSE calculations confirm (not shown) the PT prediction that swapping the pulse helicities always results in two (irreversible or reversible) spiral patterns that are mirror images of each other.

As the linear spectral phase in the TDP (14) decreases with increasing the time delay τ when $\Delta\xi < 0$, there exists a critical time delay,

$$\tau_c = -\tau_0^2 \omega_0 \Delta\xi / 4 \ln 2, \tag{15}$$

for which the linear spectral phase vanishes. When this happens the linear spectral phase components originating from the time delay and chirp balance each other. As the linear spectral phase is completely eliminated from the TDP (14), this scheme allows us to isolate a pattern purely stemming from the quadratic spectral phase $\epsilon^2 \equiv (E + E_b)^2$. Such a pattern is shown in Fig. 3(d) for the illustrative case of oppositely circularly polarized pulses with central carrier frequency $\omega_0 = 36$ eV, duration (FWHM) of $\tau_0 = 243$, as with equal and opposite chirp rates of $\xi_1 = -\xi_2 = -1$, for which the critical time delay evaluates to $\tau_c = 1.165$ fs. For these laser parameters, one observes a counterclockwise irreversible spiral pattern that is tightly wound because the spectral phase ϵ^2 has a linear term ($\propto 2E_bE$) and a quadratic term $\propto E^2$, but this time with the same sign. For the values of the time delay used in Fig. 3, the shapes of the electric field components in the polarization plane are such that the notion of slit is not applicable for Figs. 3(a) and 3(c), while it is applicable for Figs. 3(b) and 3(d).

For the relatively weak intensity used throughout this work, the numerical TDSE results (including the total electric field) confirm qualitatively all the predictions by PT. Recall that our PT is based on the RWA (excluding the c.c. part of the electric field) and on the assumption that the ground-state depletion by the first pulse is negligible in the case of time-delayed laser pulses. For a quantitative confirmation, a hybrid analytical calculation for helium atom can be done where the radial matrix element $\Upsilon(p)$ [see Eq. (10)] between the ground state and final state can be extracted numerically from a TDSE calculation by a single laser pulse that is circularly polarized. This extraction is only possible within the RWA. Indeed, the second term in Eq. (14) of Ref. [63] describing a photoemission process can be dropped under the RWA. Because the squared modulus of the reduced Eq. (14) in Ref. [63] for circular polarization in the polarization plane (directly proportional to $|\Upsilon(p)|^2$) equals the triply differential probability obtained from TDSE calculation by such a single laser pulse, such extraction becomes trivial. When the numerically extracted $\Upsilon(p)$ is then used in Eq. (9) or Eq. (12) to numerically calculate the corresponding PMDs, we find that the PMDs either from the complete TDSE calculation or from this hybrid analytical calculation coincide.

IV. SUMMARY AND CONCLUSIONS

In summary, using both first-order time-dependent perturbation theory and full-dimensional TDSE calculations, we studied photoionization of an S-state atom by a pair of

oppositely circularly polarized attopulses arbitrarily chirped and eventually delayed in time. We showed that two synchronous pulses linearly chirped at different rates impart a novel spectral phase to the pair of electron wave packets created simultaneously. For this linear (in intensity) ionization process by one-photon absorption, this spectral phase includes a linear term and quadratic term, which is then reflected in the photoelectron momentum distribution in the polarization plane by producing a reversible spiral pattern at zero time delay. An exquisite control of reversible spirals was achieved by varying either the time delay or the chirp rates. We demonstrated how time-delayed attopulses can be used to tune the chirp-induced linear spectral phase, thus isolating effects of a purely quadratic spectral phase or manipulating the symmetrical mirroring phenomena. All these results indicate that timing information in photoionization such as Ramsey delay can be masked by this chirp-induced spectral phase.

ACKNOWLEDGMENTS

This work is supported by the U.S. Department of Energy (DOE), Office of Science, Basic Energy Sciences (BES), under Award No. DE-SC0021054. Computations were done using Stampede 2 at TACC under Grant No. PHY-120003. This work was completed utilizing Crane and Swan of the Holland Computing Center of the University of Nebraska, which receives support from the Nebraska Research Initiative.

[1] N. F. Ramsey, A molecular beam resonance method with separated oscillating fields, Phys. Rev. **78**, 695 (1950).

[2] L. D. Noordam, D. I. Duncan, and T. F. Gallagher, Ramsey fringes in atomic Rydberg wave packets, Phys. Rev. A **45**, 4734 (1992).

[3] P. Szriftgiser, D. Guery-Odelin, M. Arndt, and J. Dalibard, Atomic wave diffraction and interference using temporal slits, Phys. Rev. Lett. **77**, 4 (1996).

[4] M. Strehle, U. Weichmann, and G. Gerber, Femtosecond time-resolved Rydberg wave-packet dynamics in two-electron system calcium, Phys. Rev. A **58**, 450 (1998).

[5] M. Wollenhaupt, A. Assion, D. Liese, Ch. Sarpe-Tudoran, T. Baumert, S. Zamith, M. A. Bouchene, B. Girard, A. Flettner, U. Weichmann, and G. Gerber, Interferences of ultrashort free electron wave packets, Phys. Rev. Lett. **89**, 173001 (2002).

[6] F. Lindner, M. G. Schatzel, H. Walther, A. Baltuska, E. Goulielmakis, F. Krausz, D. B. Milosevic, D. Bauer, W. Becker, and G. G. Paulus, Attosecond double-slit experiment, Phys. Rev. Lett. **95**, 040401 (2005).

[7] T. Remetter, P. Johnsson, J. Mauritsson, K. Varju, Y. Ni, F. Lepine, E. Gustafsson, M. Kling, J. Khan, R. Lopez-Martens, K. J. Schafer, M. J. J. Vrakking, and A. L'Huillier, Attosecond electron wave packet interferometry, Nat. Phys. **2**, 323 (2006).

[8] E. Mansten, J. M. Dahlström, J. Mauritsson, T. Ruchon, A. L'Huillier, J. Tate, M. B. Gaarde, P. Eckle, A. Guandalini, M. Holler *et al.*, Spectral signature of short attosecond pulse trains, Phys. Rev. Lett. **102**, 083002 (2009).

[9] L.-Y. Peng and A. F. Starace, Attosecond pulse carrier-envelope phase effects on ionized electron momentum and energy distributions, Phys. Rev. A **76**, 043401 (2007).

[10] J. M. Ngoko Djiokap, S. X. Hu, L. B. Madsen, N. L. Manakov, A. V. Meremianin, and A. F. Starace, Electron vortices in photoionization by circularly polarized attosecond pulses, Phys. Rev. Lett. **115**, 113004 (2015).

[11] J. M. Ngoko Djiokap, A. V. Meremianin, N. L. Manakov, S. X. Hu, L. B. Madsen, and A. F. Starace, Multistart spiral electron vortices in ionization by circularly polarized UV pulses, Phys. Rev. A **94**, 013408 (2016).

[12] D. Pengel, S. Kerbstadt, D. Johannmeyer, L. Englert, T. Bayer, and M. Wollenhaupt, Electron vortices in femtosecond multiphoton ionization, Phys. Rev. Lett. **118**, 053003 (2017).

[13] D. Pengel, S. Kerbstadt, L. Englert, T. Bayer, and M. Wollenhaupt, Control of three-dimensional electron vortices from femtosecond multiphoton ionization, Phys. Rev. A **96**, 043426 (2017).

[14] J. M. Ngoko Djiokap, Atomic photoionization by multiple temporal pairs of slits, Phys. Rev. A **104**, 013115 (2021).

[15] P. M. Paul, E. S. Toma, P. Breger, G. Mullot, F. Augé, Ph. Balcou, H. G. Muller, and P. Agostini, Observation of a train of attosecond pulses from high harmonic generation, Science **292**, 1689 (2001).

[16] M. Hentschel, R. Kienberger, C. Spielmann, G. A. Reider, N. Milosevic, T. Brabec, P. Corkum, U. Heinzmann, M. Drescher, and F. Krausz, Attosecond metrology, Nature (London) **414**, 509 (2001).

[17] G. Sansone, E. Benedetti, F. Calegari, C. Vozzi, L. Avaldi, R. Flammini, L. Poletto, P. Villoresi, C. Altucci, R. Velotta, S. Stagira, S. De Silvestri, and M. Nisoli, Isolated single-cycle attosecond pulses, Science **314**, 443 (2006).

[18] E. Goulielmakis, M. Schultze, M. Hofstetter, V. S. Yakovlev, J. Gagnon, M. Uiberacker, A. L. Aquila, E. M. Gullikson, D. T. Attwood, R. Kienberger, F. Krausz, and U. Kleineberg, Single-cycle nonlinear optics, Science **320**, 1614 (2008).

[19] S. Gilbertson, Y. Wu, S. D. Khan, M. Chini, K. Zhao, X. Feng, and Z. Chang, Isolated attosecond pulse generation using multicycle pulses directly from a laser amplifier, Phys. Rev. A **81**, 043810 (2010).

[20] K. Zhao, Q. Zhang, M. Chini, Y. Wu, X. Wang, and Z. Chang, Tailoring a 67 attosecond pulse through advantageous phase-mismatch, Opt. Lett. **37**, 3891 (2012).

[21] P.-C. Huang, C. Hernández-García, J.-T. Huang, P.-Y. Huang, C.-H. Lu, L. Rego, D. D. Hickstein, J. L. Ellis, A. Jaron-Becker, A. Becker *et al.*, Polarization control of isolated high-harmonic pulses, Nat. Photonics **12**, 349 (2018).

[22] J. Duris, S. Li, T. Driver, E. G. Champenois, J. P. MacArthur, A. A. Lutman, Z. Zhang, P. Rosenberger, J. W. Aldrich, R. Coffee *et al.*, Tunable isolated attosecond x-ray pulses with gigawatt peak power from a free-electron laser, Nat. Photonics **14**, 30 (2020).

[23] M. Nisoli, P. Decleva, F. Calegari, A. Palacios, and F. Martín, Attosecond electron dynamics in molecules, Chem. Rev. **117**, 10760 (2017).

[24] D. Mathur and F. A. Rajgara, Dissociative ionization of methane by chirped pulses of intense laser laser light, J. Chem. Phys. **120**, 5616 (2004).
[25] T. Nakajima, Above-threshold ionization by chirped laser pulses, Phys. Rev. A **75**, 053409 (2007).
[26] T. Nakajima and E. Cormier, Effects of the carrier-envelope phase of chirped laser pulses in the multiphoton ionization regime, Opt. Lett. **32**, 2879 (2007).
[27] T.-G. Lee, M. S. Pindzola, and F. Robicheaux, Energy and angular differential probabilities for photoionization of He using chirped attosecond soft-x-ray pulses, Phys. Rev. A **79**, 053420 (2009).
[28] M. J. Abel, T. Pfeifer, A. Jullien, P. M. Nagel, M. J. Bell, D. M. Neumark, and S. R. Leone, Carrier-envelope phase-dependent quantum interferences multiphoton ionization, J. Phys. B **42**, 075601 (2009).
[29] Y. Xiang, Y. Niu, and S. Gong, Above-threshold ionization by few-cycle nonlinear chirped pulses, Phys. Rev. A **80**, 023423 (2009).
[30] L.-Y. Peng, F. Tan, Q. Gong, E. A. Pronin, and A. F. Starace, Few-cycle attosecond pulse chirp effects on asymmetries in ionized electron momentum distributions, Phys. Rev. A **80**, 013407 (2009).
[31] M. Krug, T. Bayer, M. Wollenhaupt, C. Sarpe-Tudoran, T. Baumert, S. S. Ivanov, and N. V. Vitanov, Coherent strong-field control of multiple states by a single chirped femtosecond laser pulse, New J. Phys. **11**, 105051 (2009).
[32] P. Horsch, G. Urbasch, K.-M. Weitzel, and D. Kröner, Circular dichroism in ion yields employing femtosecond laser ionization–The role of the laser pulse duration, Phys. Chem. Chem. Phys. **13**, 2378 (2011).
[33] E. A. Pronin, A. F. Starace, and L.-Y. Peng, Perturbation-theory analysis of ionization by a chirped few-cycle attosecond pulse, Phys. Rev. A **84**, 013417 (2011).
[34] S. Laulan, J. Hache, H. S. Ba, and S. Barmaki, Ionization process of atoms by intense femtosecond chirped laser pulses, J. Mod. Phys. **04**, 20 (2013).
[35] J. R. Gulley and T. E. Lanier, Model for ultrashort laser pulse-induced ionization dynamics in transparent solids, Phys. Rev. B **90**, 155119 (2014).
[36] S. Barmaki, P. Lanteigne, and S. Laulan, Control of two-photon double ionization of helium with intense chirped attosecond laser pulses, Phys. Rev. A **89**, 063406 (2014).
[37] D. Zille, D. Adolph, M. Möller, A. M. Sayler, and G. G. Paulus, Chirp and carrier-envelope-phase effects in the multiphoton regime: Measurements and analytical modeling o strong-field ionization of sodium, New J. Phys. **20**, 063018 (2018).
[38] B. Kaufman, T. Rozgonyi, P. Marquetand, and T. Weinacht, Competition between dynamic resonance and internal conversion in strong-field molecular ionization with chirped ultrafast laser pulses, Phys. Rev. A **103**, 023108 (2021).
[39] F. Zhu, X. Liu, Y. Gao, N. Wang, L. Jiao, and A. Liu, Chirp-dependent ionization of hydrogen atoms in the presence of super-intense laser pulses, Chin. Phys. B **30**, 094209 (2021).
[40] S. Li, B. Jochim, J. Stamm, D. Peng, H.-C. Shao, J. M. Ngoko Djiokap, and M. Dantus, Pulse shaping in strong-field ionization: Theory and experiments, Phys. Rev. A **105**, 053105 (2022).
[41] V. Schäfer, and K.-M. Weitzel, Qualitative and quantitative distinction of ortho-, meta-, and para-fluorescence by means of chirped femtosecond laser ionization, Anal. Chem. **92**, 5492 (2020).
[42] G. L. Yudin, A. D. Bandrauk, and P. B. Corkum, Chirped attosecond photoelectron spectroscopy, Phys. Rev. Lett. **96**, 063002 (2006).
[43] N. J. Strandquist, Jr., and J. M. Ngoko Djiokap, Reversible electron spirals by chirped attopulses at zero time delay, Phys. Rev. A **106**, 043110 (2022).
[44] M. Wollenhaupt (private communication).
[45] M. Wollenhaupt, A. Assion, and T. Baumert, *Femtosecond Laser Pulses: Linear Properties, Manipulation, Generation and Measurement, Springer Handbook of Laser and Optics* (Springer Science & Business Media, New York, 2007), Chap. 12.
[46] T. Csizmadia, L. G. Oldal, P. Ye, S. Majorosi, P. Tzallas, G. Sansone, V. Tosa, K. Varjú, B. Major, and S. Kahaly, Detailed study of quantum path interferences in high harmonic generation driven by chirped laser pulses, New J. Phys. **23**, 123012 (2021).
[47] Z. Chang, *Fundamentals of Attosecond Optics* (CRC Press, Boca Raton, FL, 2011).
[48] M. S. Pindzola and F. Robicheaux, Total ionization cross section for electron-hydrogen scattering using a time-dependent close-coupling method, Phys. Rev. A **54**, 2142 (1996).
[49] M. S. Pindzola and F. Robicheaux, Time-dependent close-coupling calculations of correlated photoionization processes in helium, Phys. Rev. A **57**, 318 (1998).
[50] C. W. McCurdy, M. Baertschy, and T. N. Rescigno, Solving the three-body Coulomb breakup problem using exterior complex scaling, J. Phys. B **37**, R137 (2004).
[51] S. X. Hu, Optimizing the FEDVR-TDCC code for exploring the quantum dynamics of two-electron systems in intense laser pulses, Phys. Rev. E **81**, 056705 (2010).
[52] J. M. N. Djiokap, S. X. Hu, W.-C. Jiang, L.-Y. Peng, and A. F. Starace, Enhanced asymmetry in few-cycle attosecond pulse ionization of He in the vicinity of autoionizing resonances, New J. Phys. **14**, 095010 (2012).
[53] J. M. Ngoko Djiokap, S. X. Hu, W.-C. Jiang, L.-Y. Peng, and A. F. Starace, Asymmetries in production of $He^+(n = 2)$ with an intense few-cycle attosecond pulse, Phys. Rev. A **88**, 011401(R) (2013).
[54] J. M. Ngoko Djiokap, N. L. Manakov, A. V. Meremianin, and A. F. Starace, Carrier-envelope-phase-induced asymmetries in double ionization of helium by an intense few-cycle XUV pulse, Phys. Rev. A **88**, 053411 (2013).
[55] T. K. Kjeldsen, L. A. A. Nikolopoulos, and L. B. Madsen, Solving the m-mixing problem for the three-dimensional time-dependent Schrödinger equation by rotations: Application to strong-field ionization of H_2^+, Phys. Rev. A **75**, 063427 (2007).
[56] H. G. Muller, An efficient propagation scheme for the time-dependent Schrödinger equation in the velocity gauge, Laser Phys. **9**, 138 (1999).
[57] J. M. Ngoko Djiokap, N. L. Manakov, A. V. Meremianin, S. X. Hu, L. B. Madsen, and A. F. Starace, Nonlinear dichroism in back-to-back double ionization of He by an intense elliptically polarized few-cycle extreme ultraviolet pulse, Phys. Rev. Lett. **113**, 223002 (2014).

[58] J. M. Ngoko Djiokap, A. V. Meremianin, N. L. Manakov, S. X. Hu, L. B. Madsen, and A. F. Starace, Kinematical vortices in double photoionization of helium by attosecond pulses, Phys. Rev. A **96**, 013405 (2017).

[59] J. M. Ngoko Djiokap and A. F. Starace, Doubly-excited state effects on two-photon double ionization of helium by time-delayed, oppositely circularly-polarized attosecond pulses, J. Opt. **19**, 124003 (2017).

[60] L. B. Madsen, L. A. A. Nikolopoulos, T. K. Kjeldsen, and J. Fernandez, Extracting continuum information from $\Psi(t)$ in time-dependent wave-packet calculations, Phys. Rev. A **76**, 063407 (2007).

[61] A. S. Davydov, *Quantum Mechanics*, 2nd ed. (Pergamon Press, Oxford, 1976).

[62] A. F. Starace, *Theory of Atomic Photoionization, Hand-buch der Physik*, Edited by W. Mehlhorn (Springer-Verlag, Berlin, 1982), Vol. 31, pp. 1–121.

[63] E. A. Pronin, A. F. Starace, M. V. Frolov, and N. L. Manakov, Perturbation-theory analysis of attosecond photoionization, Phys. Rev. A **80**, 063403 (2009).